Studies of a Rapid Change Detector Using CYGNSS Level-2 Wind Speed Products

Mohammad M. Al-Khaldi, *Member, IEEE*, Alexandra Bringer, *Member, IEEE*, and Joel T. Johnson, *Fellow, IEEE*

***Abstract*—This work further investigates the use of ocean wind speed retrievals from NASA's Cyclone Global Navigation Satellite System (CYGNSS) mission that are closely spaced in space and in time to detect regions in the atmosphere undergoing "rapid" change. As in a previous investigation, CYGNSS measurement "clumps" (i.e., groups of wind speed measurements satisfying specified time/space separation criteria) are used to create a wind speed change detector, and the results are compared to a set of atmospheric properties derived from Modern-Era Retrospective Analysis for Research and Applications 2 model datasets. The analysis uses a four-year CYGNSS Level-2 wind speed dataset developed by the National Oceanic and Atmospheric Administration and highlights the potential for using CYGNSS's wind speed measurements to locate various dynamic activities occurring over the ocean's surface. The presented results also highlight some of the challenges of the method, including the inherent dependence of detection performance on the quality of CYGNSS's wind speed estimates as well as the validity of comparisons to "truth" datasets having temporal resolutions much coarser than those provided by CYGNSS.**

***Index Terms*—Bistatic radar systems, cyclone global navigation satellite system (CYGNSS), global navigation satellite systems reflectometry (GNSS-R), ocean surface dynamics, rough surface scattering.**

I. Introduction

THE detection of highly dynamic regions of the atmosphere (for example, along fronts, cyclones, or in other convective regions) is key for improved understanding and prediction of the genesis of frontal wave cyclones, extreme surface temperature shifts, heavy precipitation, and maintaining an understanding of the central components that influence the Earth's weather [1]–[4]. A wide range of definitions may be used to characterize "highly dynamic regions" that are here taken as characterized by high spatial gradients over time scales that range from the very short (subhour level) to systems that occur over periods of 1–6 h. The varied spatial and temporal scales over which such features can occur make their remote sensing using spaceborne platforms desirable. NASA's Cyclone Global Navigation Satellite System (CYGNSS) mission appears well suited to address this need given its extensive coverage (latitudes $-38^\circ \leq \varphi \leq 38^\circ$) focused on tropical regions, where a significant fraction of Earth's deep atmospheric convection occurs [5] as well as its eight satellite constellation that provides 7 and 3 h mean and median revisit times, respectively [6], [7].

This article expands on a previous investigation [8] on the use of CYGNSS's revisit characteristics to detect dynamic atmospheric regions over the ocean's surface. In this work, the method used in [8] to define CYGNSS measurement "clumps" within which detections are performed is revised by adopting a dynamic approach that is better adapted to the nature of CYGNSS measurements. The detection procedure is also revised from that of [8] by implementing an adaptive detection process that defines clump-specific detection thresholds. While a complete assessment of the method is challenged by the absence of large-scale model datasets that resolve on the subhour time scales considered, results are shown that illustrate the features detected as a function of the detection threshold applied. In general, the method is shown to be capable of providing information on dynamic atmospheric regions as associated, for example, with cyclonic activity, land–atmosphere–ocean exchanges, and atmospheric turbulence.

The next section provides an overview of CYGNSS's basic operation and data products. Section III then reviews the novel properties of CYGNSS's ocean surface spatiotemporal sampling patterns, the definition of CYGNSS measurement clumps, and the proposed convective activity detection methodology. A brief overview of the reference datasets used in this work is also provided. Section IV then reports results using a four-year CYGNSS dataset and provides both quantitative and qualitative assessments of detection performance. Particular emphasis is placed on the tradeoffs in terms of detection probabilities and false alarm rates associated with the enforcement of a wide range of detection thresholds when compared to "truth" fields adopted from the MERRA-2 model. Section V then provides a summary of the results and recommendations for future work.

II. Background

A. CYGNSS Operation and Data Products

The CYGNSS mission operates a constellation of eight satellites in low Earth orbit. The primary scientific payload of each

Manuscript received March 13, 2021; revised July 22, 2021; accepted July 28, 2021. Date of publication August 4, 2021; date of current version August 19, 2021. This work was supported in part by NASA ROSES 2016 Weather Program under Grant NNH16ZDA001N-WEATHER and in part by an allocation of computing resources from the Ohio Supercomputer Center. *(Corresponding author: Mohammad M. Al-Khaldi.)*

Mohammad M. Al-Khaldi is with the Constellation Observing System for Meteorology, Ionosphere, and Climate Program, University Corporation for Atmospheric Research, Boulder, CO 80301 USA (e-mail: malkhaldi@ucar.edu).

Alexandra Bringer and Joel T. Johnson are with the Department of Electrical and Computer Engineering and the ElectroScience Laboratory, The Ohio State University, Columbus, OH 43210 USA (e-mail: bringer.1@osu.edu; johnson.1374@osu.edu).

Digital Object Identifier 10.1109/JSTARS.2021.3101500

of the satellites is the delay-Doppler mapping instrument that receives GPS signals reflected from Earth's surface [9]. By cross correlating received GPS transmissions with a locally generated copy of the transmitted GPS C/A-code, the fundamental GNSS-R measurement, the delay-Doppler map (DDM), is formed. "Pixels" in the DDM represent the power scattered from Earth's surface at specific offsets in delay and Doppler from the specular reflection point.

The CYGNSS mission provides three levels of data products; the proposed detection methodology uses Level-2 (L2) wind speed estimates. An L2 wind speed estimate is obtained from a normalized radar cross section (NRCS) value derived from a DDM measurement using the DDM average [10], [11] defined as an integration of the bistatic radar cross section within a predefined delay-Doppler window about the specular DDM bin normalized by the effective scattering area. NRCS values are regressed against wind speeds provided by other instruments and/or models to derive a geophysical model function (GMF) for converting the NRCS into wind speed. Fundamentally, the GMF is, therefore, a function that expects an NRCS or a related observable quantity (trailing edge slope, for example) as its input, as well as other information on the measurement configuration (incidence angle, etc.), and provides wind speed estimates as its output. A more comprehensive overview of the factors dictating the formulation and tuning of the CYGNSS GMFs is provided in [12].

While standard CYGNSS wind products continue to advance, the difficulties of achieving precise power calibration [14] across all eight observatories together with the variability that GPS power flexing events [15] cause have motivated investigating means with which the quality of CYGNSS ocean surface wind estimates may be improved. The studies of this article are particularly sensitive to any biases among CYGNSS observatories, since measurement clumps may include wind speed estimates obtained from differing satellites in the constellation, making use of products that eliminate such biases important for improving performance. The National Oceanic and Atmospheric Administration (NOAA) L2 wind (u_{10}^{N}) product addresses these challenges by introducing a correction term for each CYGNSS measurement "track" that minimizes the bias for the entire track when compared to predicted CYGNSS measurements using European Centre for Medium-Range Weather Forecasts [16] wind speeds. The single correction applied for each track represents an average over up to several hundred specular points extending up to several thousand kilometers in length, which limits the influence of the model to the correction of CYGNSS measurement biases between tracks and/or observatories. Due to these desirable properties, the L2 wind speed estimates of the NOAA v1.1 product are used in this work.

III. Rapid Variability Detection Methodology

A. Clump Definition

CYGNSS's measurements occur as individual specular points within a track that represents a particular GPS transmitter/CYGNSS receiver combination. Due to the complex nature of the combined CYGNSS and GPS satellite orbits, CYGNSS coverage occurs in an irregular pattern, making statistical descriptions such as the 7 and 3 h mean and median revisit times useful. These statistics, however, vary with latitude, and shorter revisits at subhourly rates regularly occur as the constellation overpasses a given location. It is also noted that the spatial grid, within which a revisit is defined, influences these results; the nominal spatial resolution of a CYGNSS measurement is approximately 25 km.

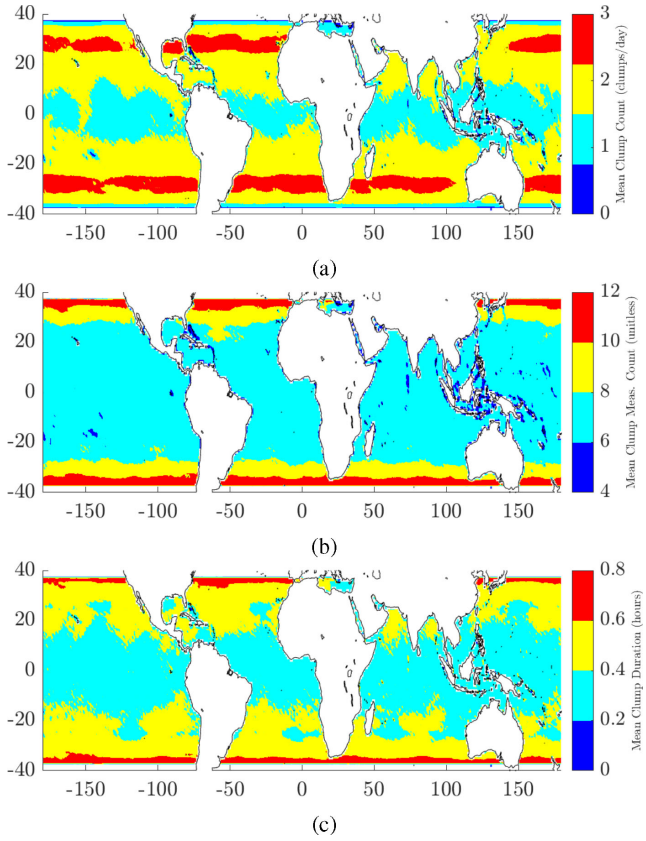

Fig. 1. Clump statistics using CYGNSS L2 wind estimates obtained over 2017–2020. (a) Mean number of clumps per day. (b) Mean number of measurements forming a clump. (c) Mean clump duration.

The proposed detection methodology examines the variability in wind speed estimates within a "clump" to flag locations experiencing dynamic activity.

CYGNSS measurement clumps are defined first by gridding NOAA v1.1 wind speed estimates onto a daily 1° by 1° lat/lon grid. The daily time series in each grid cell is then examined to identify gaps between successive measurements of greater than 1 h duration. Clumps are then defined as groups of measurements between these "gap" periods. In order to be retained for further analysis, a clump must have a minimum of three wind speed estimates. The average number of estimates per clump following these procedures was found to be 8, and the average clump duration was 21.94 min. This approach adapts the "static" method used in [8] (which used fixed clump durations) into a "dynamic" definition that is more suited to the varying revisit properties obtained from CYGNSS as a function of latitude. Fig. 1 illustrates clump statistics over the period of interest, including the mean number of clumps identified per

day (upper plot), the mean number of measurements within a clump (middle), and the mean duration of a clump (lower). The latitude-dependent nature of these quantities is evident, as well as the ability of CYGNSS to provide multiple measurements within subhour time periods. The performance of the proposed method for detecting atmospheric dynamics should also, therefore, be expected to be latitude dependent.

B. Detector

Rapid change detection is performed by applying a threshold to the variance of wind speed estimates within a clump, since higher levels of variability within a clump indicate changes occurring either within the time duration of the measurements within the clump or within the 1° by 1° grid cell in space considered. First, consider the "false alarm" case. Wind speed estimates within clumps not experiencing rapid variability (i.e., "stationary clumps") can be modeled as a set of independent normally distributed random variables X_i

$$X_i \propto N\left(\mu, \sigma^2\right) = \mu + \sigma N(0,1) \tag{1}$$

where μ is the mean wind speed and σ is the measurement error. The wind speed variance within a clump of N_c samples can then be estimated as

$$V = \frac{1}{N_c - 1} \sum_{i=1}^{N_c} (X_i - \tilde{\mu})^2 \tag{2}$$

where $\tilde{\mu}$ is the sample mean. From (2), it follows that the variance estimator V has a scaled chi-squared distribution with $N_c - 1$ degrees of freedom ($\chi^2_{N_c-1}$) with $\langle V \rangle = \sigma^2$ and variance

$$\mathrm{Var}(V) = \frac{2\sigma^4}{N_c - 1} N_c. \tag{3}$$

A detection threshold V_{thresh} on the sample variance V can be specified based on the probability I_{fa} that a stationary clump's wind variance exceeds the threshold

$$I_{\text{fa}} = P(V > V_{\text{thresh}}) = 1 - \chi^2_{N_c-1,\text{cdf}}\left(\frac{N_c - 1}{\sigma^2} V_{\text{thresh}}\right). \tag{4}$$

Here, $\chi^2_{N_c-1,\text{cdf}}$ is the cumulative distribution function of a standard chi-squared random variable. While estimating the uncertainties associated with CYGNSS retrievals is complicated by their wind speed dependence, in what follows, a value of 1.67 m/s is used to approximate CYGNSS's measurement error based on previous assessments of CYGNSS's L2 wind speed error properties [17], [18]. Using (4) and the specified value for σ^2, estimates of V_{thresh} corresponding to specified false alarm rates I_{fa} and the number of samples within a clump N_c can be determined, as shown in Fig. 2. This approach for determining the threshold improves that of [8] (in which a fixed V_{thresh} value was used) by attempting to retain a fixed false alarm rate as N_c varies. However, it should be expected that detection performance will remain dependent on the number of samples within a clump. In addition, results when comparing CYGNSS "detections" from those obtained from meteorological models will be dependent on a wide range of additional factors, so that the specified I_{fa} value will not precisely specify the eventual "false alarm" rate in such comparisons.

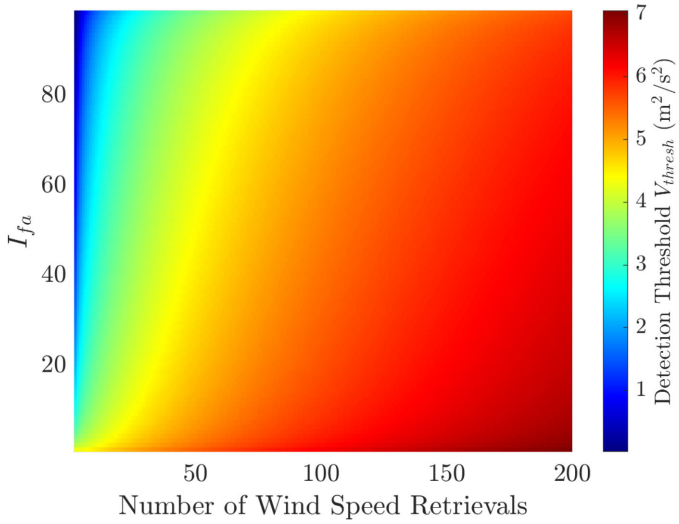

Fig. 2. V_{thresh} as a function of N_c (number of measurements within a clump) and I_{fa} (probability that the variance estimate V exceeds threshold in the stationary clump case).

C. Reference Datasets

To provide quantitative and qualitative comparisons with detector results, the Modern-Era Retrospective Analysis for Research and Applications 2 (MERRA-2) dataset is used as a reference. The wind speeds provided by MERRA-2 w_{10} are used to compute, over the duration of a given clump, the magnitude of the wind speed gradient $|\nabla w_{10}|$, which is here used as a proxy indicator of dynamic behavior. As with the threshold on wind speed variance within a clump, a threshold is invoked on the MERRA-2 $|\nabla w_{10}|$ value to indicate locations of interest. Fig. 3 illustrates detection locations for thresholds ranging from smaller (upper plot) to moderate (middle) to larger (lower plot) values of 0.007, 0.045, and 0.14 m $\cdot$ s$^{-1}\cdot$km^{-1}, respectively. Given the fraction of detected pixels of 60%, 10%, and 0.01% for these thresholds, respectively, a value of 0.045 was selected as providing a more realistic representation of the locations, patterns, and relative prevalence of dynamic locations as compared to previously reported indicators [8]. Points detected using the 0.045 threshold are used for comparison in Section IV.

It is noted that this comparison is only one of many possibilities, and that intercomparisons between the CYGNSS- and MERRA-2-derived quantities should be carefully interpreted. MERRA-2 winds are a reanalysis product that is produced on an hourly basis and, thus, may not consistently capture the variability that can occur on the finer time scales within a CYGNSS clump. Furthermore, the MERRA-2 product assimilates millions of observations [19] from a variety of platforms over a given wind field cycle, all of which undergo a process of recursive filtering, which promotes spatial homogeneity and smooth wind field variations in all directions [20]. While this process significantly improves the quality of the final wind field products, for the purposes of this study, it may also have the

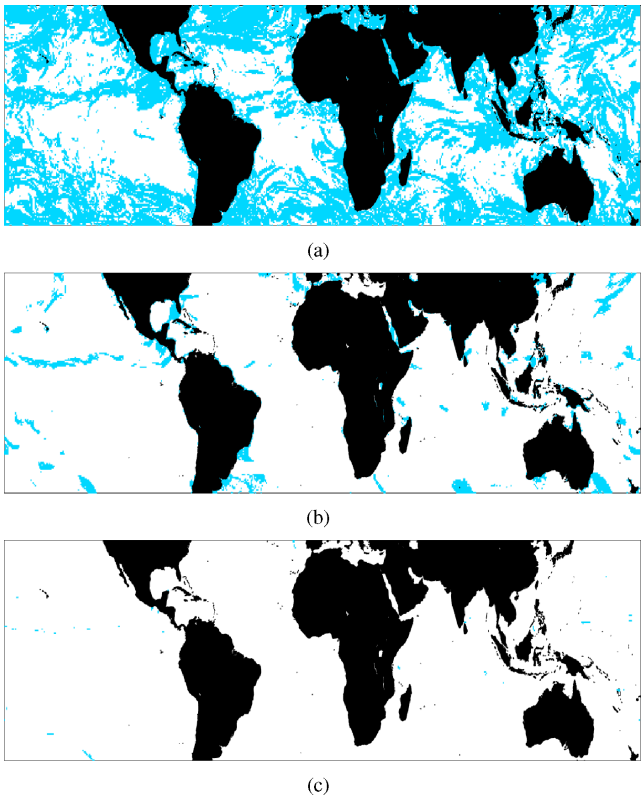

Fig. 3. Examples of MERRA-2 reference frontal boundary declarations (in cyan) at wind gradient thresholds of (a) 0.007 m · s^{-1}·km^{-1}, (b) 0.045 m· s^{-1}·km^{-1}, and (c) 0.14 m· s^{-1}·km^{-1}.

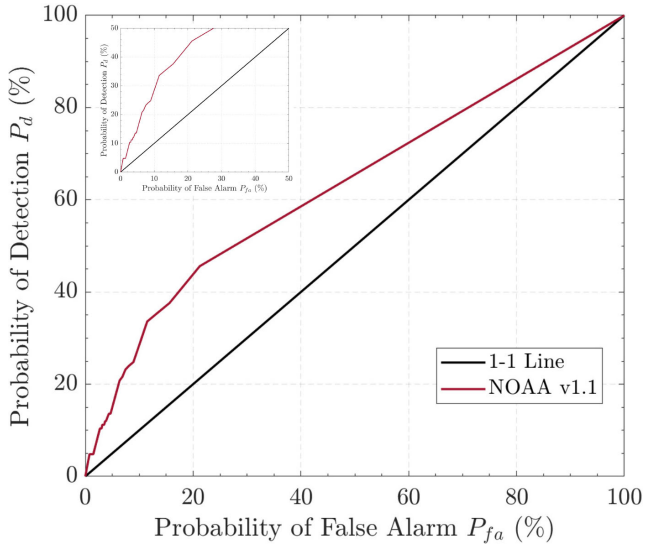

Fig. 4. Standard ROC curve setting MERRA-2 detections as "truth" at $|\nabla w_{10}|$ = 0.045-m · s^{-1}·km^{-1} threshold. Analysis uses all NOAA L2 wind speed estimates from DOY 121, 2017 to DOY 366, 2020. The insert is an identical axis-limited ROC curve.

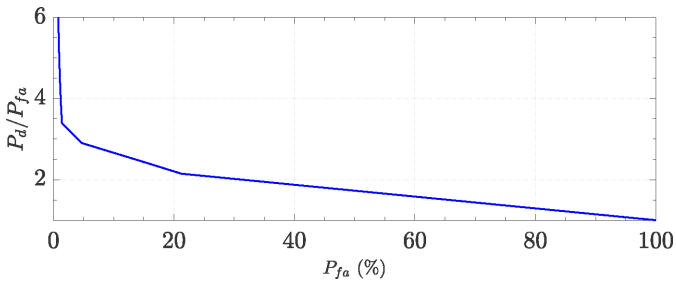

Fig. 5. Ratio of probability of detection to probability of false alarm versus probability of false alarm using all NOAA L2 wind speed estimates from DOY 121, 2017 to DOY 366, 2020.

undesired impact of dampening any anomalies associated with rapidly changing wind fields that may be included in CYGNSS measurements.

IV. Results

A. Global Detection

Adopting the MERRA-2 wind speed gradient detector with a 0.045-m · s^{-1}·km^{-1} threshold as "truth," the receiver operating characteristic (ROC) curve shown in Fig. 4 is obtained for the CYGNSS clump detector. This plot summarizes the probability of detection (i.e., both CYGNSS and MERRA-2 indicate rapid change) and the probability of false alarm (i.e., CYGNSS indicates rapid change, while MERRA-2 indicates no rapid change) as I_{fa} is varied. These results use all clumps obtained from the NOAA L2 CYGNSS wind speed products from DOY 121, 2017 to DOY 366, 2020. The obtained ROC curve is compared against the "no skill" (i.e., random choice) curve in Fig. 4; the results shown clearly illustrate the value of the CYGNSS dataset in identifying MERRA-2 high wind gradient regions. The information in Fig. 4 further provides the opportunity to identify an operating point (i.e., a particular detection probability, P_d, and false alarm rate, P_{fa}, combination) for specified applications. Fig. 5 further plots the ratio of the detection probability (P_d) to the false alarm rate (P_{fa}). While, practically, it is of particular interest to minimize P_{fa} while maximizing P_d (i.e., $P_d/P_{\text{fa}} \to \infty$), the ratio estimates in Fig. 5 show that values less than approximately 6 occur for this detector. Again, it should be recalled that the comparison performed is dependent on the nature of the CYGNSS-derived and MERRA-2-derived products.

Further analysis is provided in Fig. 6, which plots CYGNSS/MERRA-2-detected locations for January 1, 2020, on which a total of 36 633 clumps were formed having an average of nine measurements per clump with a mean clump duration of 34 min 24 s. The three plots illustrated use successively relaxed detection thresholds derived from P_{fa} values of 0%, 1%, and 22%, respectively. In the upper plot that uses detection thresholds that ensure $P_{\text{fa}} = 0\%$, a clump wind variance >13 m/s is required for detection to be declared resulting in no detections occurring. The middle plot having $P_{\text{fa}} = 1\%$ shows 5.33% of pixels detected with probability of detection 15.69% in this specific example. While the P_d estimates provided are based on a per-pixel comparison basis, comparisons with MERRA-2 detections within a 100-km radius centered about CYGNSS's detections show an increased probability of detection on the order of 40–50%. The more relaxed set of detection thresholds used as in plot (c) further increases the detection probability to 39.63%.

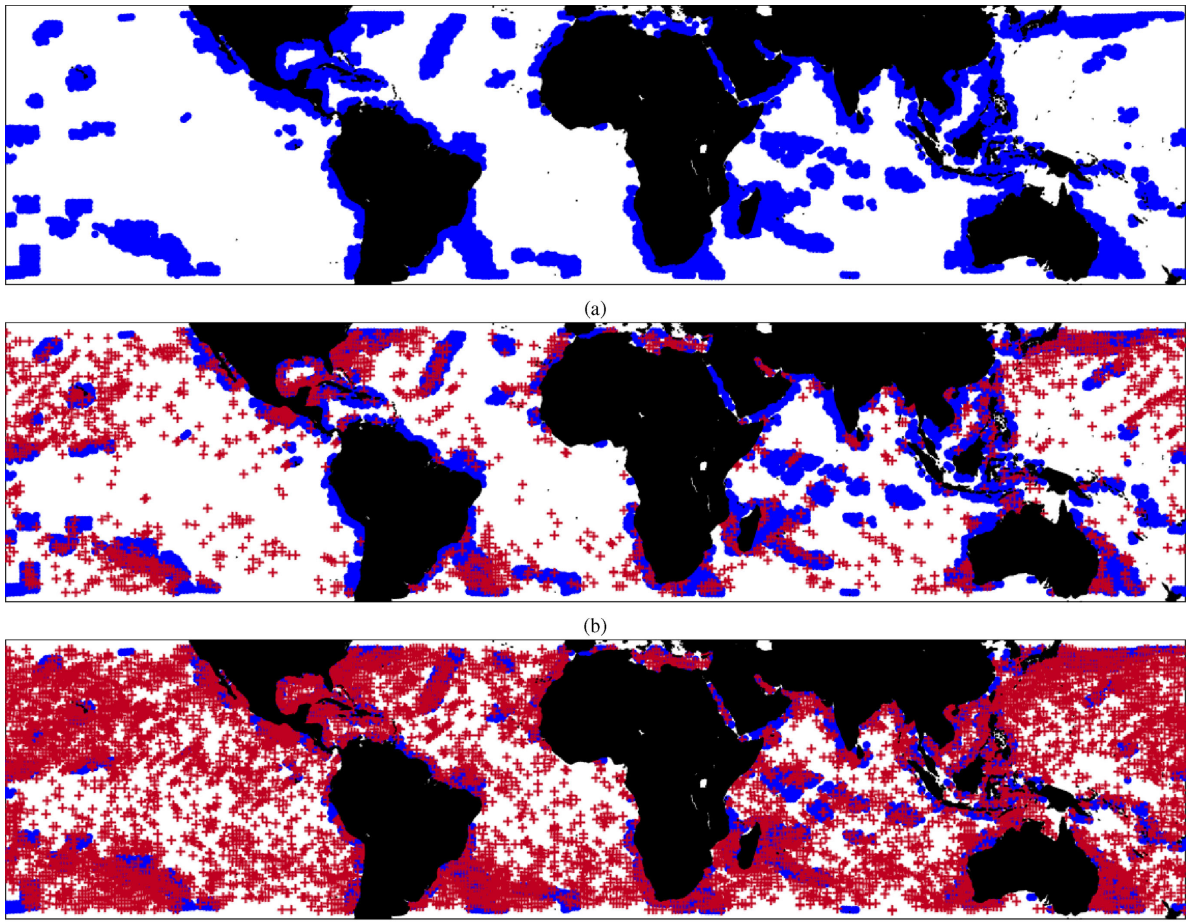

Fig. 6. Comparisons of CYGNSS versus MERRA-2 convective activity detection results for March 1, 2020. CYGNSS detections are in red, and MERRA-2 detections are in blue. The plots are produced using V_{thresh} based on false alarm rates P_{fa} rates of (a) 0%, (b) 1%, and (c) 22%.

As seen in Fig. 5, selecting intended false alarm rates less than approximately 2% can achieve P_d/P_{fa} ratios ranging from 4 to 6, indicating a reasonable detection reliability that may be sufficient for some applications, albeit at a modest probability of detection. In the case studies that follow, the detector is operated at $P_{\text{fa}} = 1\%$.

B. Example: Cyclonic Activity

The genesis and development of cyclones clearly represent regions of dynamic atmospheric change [21], [22]; the early stages of cyclonic development are of particular interest. Fig. 7 illustrates an example for Hurricane Alberto on DOY 146, 2018, which underwent an increase in its sustained surface winds from 18 m/s to a peak of 28 m/s within this 24-h period. The MERRA-2 wind speeds shown in the color scale of the left plot along with the contours marking the boundaries within which the MERRA-2 wind speed gradient indicated a detection suggest the formation of the storm's eyewall and its transition region. A concurrently detected CYGNSS clump that includes eight wind speed measurements (three from the CYG03 and five from the CYG07 observatory) shows wind speeds ranging from 6.4 to 13.7 m/s over a 9-min period within this 1° by 1° grid cell. The right plot shows the specular point locations of the clump and includes the time in minutes for each clump measurement. This high variability results in the clump being detected as experiencing dynamic activity. In this case, the variability within the clump likely corresponds to the high spatial, rather than temporal, gradient of the winds within the region examined.

C. Example: Mediterranean Sea

The Mediterranean Sea is a region known to be associated with various forms of cyclical atmospheric turbulence relating to periods of increased atmospheric dynamics bringing about heavy rain as well as the development of cyclonic systems. The cyclical nature of these phenomena provides an opportunity to compare results during periods known to have higher or lower levels of atmospheric change. As an example, Fig. 8 shows that a significantly increased number of detections occurs for both CYGNSS and MERRA-2 on January 1, 2020 as compared to May 1, 2020 (left and right plots, respectively). This is consistent with the findings of previous studies [23] that show increased dynamic activity in this region from November to February that is decreased from March to September. The ability of the proposed detection methodology to leverage CYGNSS's sensitivity

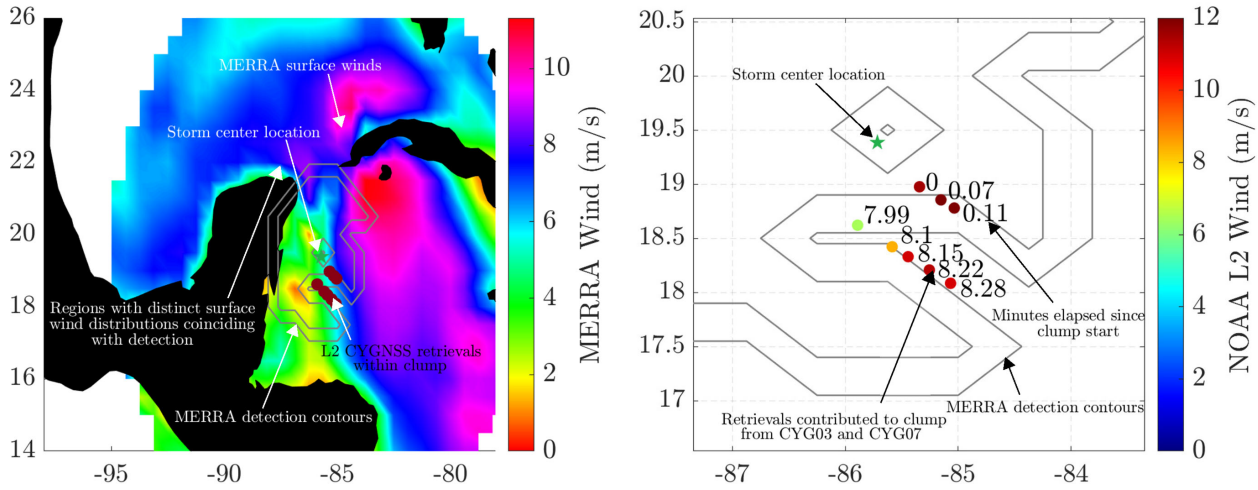

Fig. 7. Example of CYGNSS frontal boundary detection associated with hurricane development: Hurricane Alberto on DOY 146, 2018.

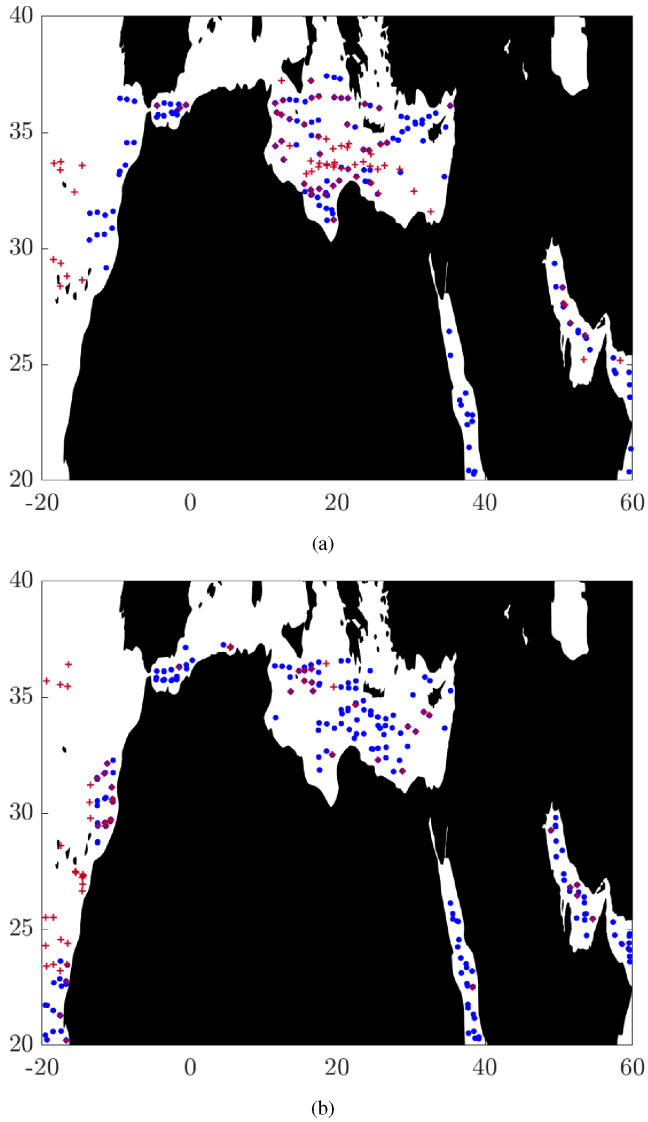

Fig. 8. Detections (CYGNSS in red, MERRA-2 in blue) in the Mediterranean Sea. (a) January 1, 2020. (b) May 1, 2020.

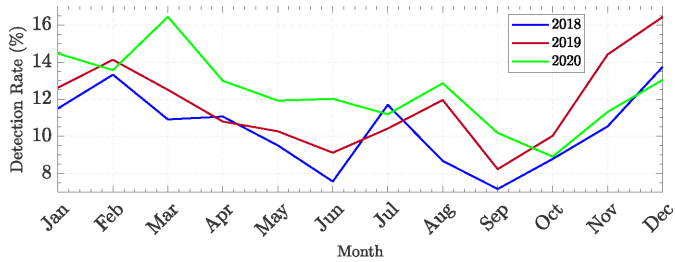

Fig. 9. Monthly time series of CYGNSS detections made in the Mediterranean Sea.

to this cyclical behavior is evidenced by the 53.13% decrease in CYGNSS detections over the two analysis periods.

A time series of the number of clumps identified to have been associated with convective activity, in the same region, relative to all clumps formed (i.e., detection rate) over the three year 2018–2020 analysis period is shown in Fig. 9. The periodicity of these events associated with increased atmospheric dynamics is evidenced by the consistent average detection rate increase of $\approx 6\%$ over the months of November–January while typically reaching its least active period over the months May–September.

V. Conclusion

This article extends the past work of [8] for detecting locations experiencing dynamic atmospheric activity through the use of CYGNSS "clump" measurements. New "dynamic" methods for defining measurement clumps and for performing detection are described. The results indicate the potential for using the proposed methodology to detect rapid variability on the ocean's surface, although comparisons with wind speed gradient magnitude-based detections from the MERRA-2 model suggest that CYGNSS-detections may require careful consideration of the detection threshold to balance the probabilities of detection and false alarm for a given application. Future work will continue development and assessment of this approach as CYGNSS wind speed products continue to be refined.

ACKNOWLEDGMENT

The authors would like to thank Center for Satellite Application and Research at National Environmental Satellite, Data, and Information Service, National Oceanographic and Atmospheric Administration (NOAA), College Park, MD, USA, for making their L2 wind speed estimates derived from the CYGNSS constellation available. The authors would like to acknowledge the NOAA for providing the NOAA v1.1 CYGNSS Level-2 wind speed product.

REFERENCES

[1] D. Parker, "Secondary frontal waves in the North Atlantic region: A dynamical perspective of current ideas," *Quart. J. Roy. Meteorol. Soc.*, vol. 124, no. 547, pp. 829–856, 1998.

[2] I. Simmonds, K. Keay, and J. T. Bye, "Identification and climatology of southern hemisphere mobile fronts in a modern reanalysis," *J. Climate*, vol. 25, no. 6, pp. 1945–1962, 2012.

[3] J. L. Catto and S. Pfahl, "The importance of fronts for extreme precipitation," *J. Geophys. Res., Atmos.*, vol. 118, no. 19, pp. 10 791–10801, 2013.

[4] J. Jenkner, M. Sprenger, I. Schwenk, C. Schwierz, S. Dierer, and D. Leuenberger, "Detection and climatology of fronts in a high-resolution model reanalysis over the Alps," *Meteorol. Appl.*, vol. 17, pp. 1–18, 2010.

[5] J. Hosking, M. Russo, P. Braesicke and J. Pyle, "Modelling deep convection and its impacts on the tropical tropopause layer," *Atmos. Chem. Phys.*, vol. 10, no. 22, pp. 11175–11188, 2010.

[6] C. Ruf *et al.*, "New ocean winds satellite mission to probe hurricanes and tropical convection," *Bull. Amer. Meteorol. Soc.*, vol. 97, no. 3, pp. 385–395, 2016.

[7] C. Bussy-Virat, C. Ruf, and A. Ridley, "Relationship between temporal and spatial resolution for a constellation of GNSS-R satellites," *IEEE J. Sel. Topics Appl. Earth Observ. Remote Sens.*, vol. 12, no. 1, pp. 16–25, Jan. 2019.

[8] J. Park, J. Johnson, Y. Yi, and A. O'Brien, "Using 'rapid revisit' CYGNSS wind speed measurements to detect convective activity," *IEEE J. Sel. Topics Appl. Earth Observ. Remote Sens.*, vol. 12, no. 1, pp. 98–106, Jan. 2019.

[9] *CYGNSS Handbook: Cyclone Global Navigation Satellite System: Deriving Surface Wind Speeds in Tropical Cyclones*. Washington, DC, USA: NASA, 2016.

[10] M. Clarizia and C. Ruf, "On the spatial resolution of GNSS reflectometry," *IEEE Geosci. Remote Sens. Lett.*, vol. 13, no. 8, pp. 1064–1068, Aug. 2016.

[11] M. Clarizia, C. Ruf, P. Jales, and C. Gommenginger, "Spaceborne GNSS-R minimum variance wind speed estimator," *IEEE Trans. Geosci. Remote Sens.*, vol. 52, no. 11, pp. 6829–6843, Nov. 2014.

[12] C. Ruf and R. Balasubramaniam, "Development of the CYGNSS geophysical model function for wind speed," *IEEE J. Sel. Topics Appl. Earth Observ. Remote Sens.*, vol. 12, no. 1, pp. 66–77, Jan. 2019.

[13] E. Uhlhorn, P. Black, J. Franklin, M. Goodberlet, J. Carswell, and A. Goldstein, "Hurricane surface wind measurements from an operational stepped frequency microwave radiometer," *Monthly Weather Rev.*, vol. 135, no. 9, pp. 3070–3085, 2007.

[14] S. Gleason, C. Ruf, A. O'Brien, and D. McKague, "The CYGNSS level 1 calibration algorithm and error analysis based on on-orbit measurements," *IEEE J. Sel. Topics Appl. Earth Observ. Remote Sens.*, vol. 12, no. 1, pp. 37–49, Jan. 2019.

[15] T. Wang, C. Ruf, B. Block, D. McKague, and S. Gleason, "Design and performance of a GPS constellation power monitor system for improved CYGNSS L1B calibration," *IEEE J. Sel. Topics Appl. Earth Observ. Remote Sens.*, vol. 12, no. 1, pp. 26–36, Jan. 2019.

[16] M. Dahoui, N. Bormann, L. Isaksen, and T. McNally, "Recent developments in the automatic checking of earth system observations," *Meteorology*, no. 162, pp 27–31, 2020.

[17] C. Ruf, S. Gleason, and D. McKague, "Assessment of CYGNSS wind speed retrieval uncertainty," *IEEE J. Sel. Topics Appl. Earth Observ. Remote Sens.*, vol. 12, no. 1, pp. 87–97, Jan. 2019.

[18] C. Ruf *et al.* "In-orbit performance of the constellation of CYGNSS hurricane satellites," *Bull. Amer. Meteorol. Soc.*, vol. 100, no. 10, pp. 2009–2023, 2019.

[19] D. Carvalho, "An assessment of NASA's GMAO MERRA-2 reanalysis surface winds," *J. Climate*, vol. 32, no. 23, pp. 8261–8281, 2019.

[20] R. Purser, W. Wu, D. Parrish, and N. Roberts, "Numerical aspects of the application of recursive filters to variational statistical analysis. Part II: Spatially inhomogeneous and anisotropic general covariances," *Monthly Weather Rev.*, vol. 131, no. 8, pp. 1536–1548, 2003.

[21] D. J. Posselt, C. M. Naud, C. Bussy-Virat, and J. A. Crespo, "Assessing CYGNSS's potential to observe extratropical fronts and cyclones," *J. Appl. Meteorol. Climatol.*, vol. 56, pp. 2027–2034, 2017.

[22] S. Dafis, J. Rysman, C. Claud, and E. Flaounas, "Remote sensing of deep convection within a tropical-like cyclone over the Mediterranean Sea," *Atmos. Sci. Lett.*, vol. 19, no. 6, 2018, Art. no. e823.

[23] B. Alhammoud, C. Claud, B. Funatsu, K. Béranger, and J. Chaboureau, "Patterns of precipitation and convection occurrence over the mediterranean basin derived from a decade of microwave satellite observations," *Atmosphere*, vol. 5, no. 2, pp. 370–398, 2014.

Mohammad M. Al-Khaldi (Member, IEEE) received the bachelor's degree in electrical engineering from the American University of Sharjah, Sharjah, United Arab Emirates, in 2015, the M.S. degree in electrical engineering from Texas A&M University, College Station, TX, USA, in 2017, and the M.S. and Ph.D. degrees in electrical and computer engineering from The Ohio State University, Columbus, OH, USA, in 2019 and 2020, respectively.

He is currently a Postdoctoral Researcher with the Constellation Observing System for Meteorology, Ionosphere, and Climate Program, University Corporation for Atmospheric Research, Boulder, CO, USA. His research interests include applied electromagnetics, rough surface scattering, and spaceborne remote sensing.

Alexandra Bringer (Member, IEEE) received the M.S. and Ph.D. degrees in physics from the Université du Sud-Toulon-Var, La Garde, France, in 2009 and 2012, respectively.

Her studies were focused on physical oceanography and remote sensing. She joined the Electroscience Laboratory, The Ohio State University, Columbus, OH, USA, in 2014. Since then, she has been working on microwave radiometry for cryosphere applications and radio frequency interference detection and mitigation. She is working with the ElectroScience Laboratory, The Ohio State University, as a Research Scientist. Her main research interests include Earth monitoring, microwave active and passive remote sensing for land, ocean, and cryosphere applications and signal processing.

Joel T. Johnson (Fellow, IEEE) received the bachelor's degree in electrical engineering from the Georgia Institute of Technology, Atlanta, GA, USA, in 1991, and the S.M. and Ph.D. degrees from the Department of Electrical Engineering and Computer Science, Massachusetts Institute of Technology, Cambridge, MA, USA, in 1993 and 1996, respectively.

He is currently a Professor with the ElectroScience Laboratory, Department of Electrical and Computer Engineering, The Ohio State University, Columbus, OH, USA. His current research interests include microwave remote sensing, propagation, and electromagnetic wave theory.

Dr. Johnson is a Member of commissions B and F of the International Union of Radio Science (URSI), Tau Beta Pi, Eta Kappa Nu, and Phi Kappa Phi. He received the 1993 Best Paper Award from the IEEE Geoscience and Remote Sensing Society, was named an Office of Naval Research Young Investigator, the National Science Foundation Career Awardee, the PECASE Award Recipient in 1997, and was recognized by the U.S. National Committee of URSI as a Booker Fellow in 2002. He was a Technical Program Co-Chair for the 2017 International Geoscience and Remote Sensing Symposium. He has served as an Associate Editor for the IEEE TRANSACTIONS ON GEOSCIENCE AND REMOTE SENSING since 2000. He is also a Past Chair of the Technical Committee on Frequency Allocations in Remote Sensing of the IEEE Geoscience and Remote Sensing Society.